

# Heat Load Experiments at CAMD and CLS

D. Yemane<sup>1</sup>, S. Achenbach<sup>2</sup>, J. Goettert<sup>1</sup>, R. Guntaka<sup>3</sup>, D. Haluzan<sup>2</sup>, K. Nandakumar<sup>3</sup>, V. Singh<sup>1</sup>,  
V. Subramanian<sup>2</sup>, G. Wells<sup>2</sup>

<sup>1</sup>LSU Center for Advanced Microstructures and Devices (CAMD), Baton Rouge, LA

<sup>2</sup>Canadian Light Source, Univ. of Saskatchewan, 101 Perimeter Road, Saskatoon, SK, Canada

<sup>3</sup>LSU-Chemical Engineering, Baton Rouge, LA

[dyemane@lsu.edu](mailto:dyemane@lsu.edu)

## Summary

Joint research described in this paper includes partners from the Canadian Light Source and LSU (CAMD, Chemical Engineering) and is built on previous work conducted by researchers at CAMD and BESSY [1]. Heat load and its impact on the patterning accuracy in deep X-ray lithography has been studied for many years and reported in a number of publications [2,3,4,5,6,7,8,9,10,11]. Investigations combine simulation and experimental results and show that thermal load can cause temperature increases ranging from a few degrees to several 10°C depending upon light source and exposure parameters. Building upon previous experiments [1] and further improvements systematic studies with a ‘worst-case scenario’ x-ray mask (100% Au coverage resulting in maximum heat load on the mask) and in-situ monitoring of temperature changes on mask and substrate during exposures were conducted. Simulation results achieved with a lumped model representing the arrangement of mask and substrate inside the scanner chamber are in good agreement and complement our experiments.

## Introduction and Background

One of the major steps in ultra-deep x-ray lithography is exposure of thick photoresists using high power synchrotron radiation such as the CAMD wiggler beamline or the SyLMAND bending magnet beamline at CLS. High energy photon x-rays make it possible to fabricate extremely tall high aspect ratio microstructures in a reasonable time. In standard LIGA fabrication, photoresists such as PMMA and SU8 are radiated with x-rays through gold patterned x-ray masks (Fig. 1a) and then developed in a liquid developer. Figure 1b shows typical patterning results using a bending magnet exposure spectrum (CAMD) into a 200µm thick PMMA resist. In this case the pattern transfer from mask to resist is very accurate and no signs of structure distortion are found. However, using high power x-ray exposure conditions at the CAMD wiggler beamline shows some pattern distortion or shift likely caused by mismatch of thermal expansion coefficient of mask and substrate.

Temperature rise during high power x-ray exposures is caused by x-ray absorption particularly in the absorber pattern of the x-ray mask which is designed to almost fully block the incident radiation. Figure 2 shows the power spectra for both CAMD and CLS source along the beamline. X-ray photons are partially blocked by matter blocking the beam such as Beryllium window (Be), optional filters, mask substrate (C), and mask absorber (Au). For both beamlines approximately 5.4 mrad of beam width is impinging onto the mask shown in Fig. 1 (open area Ø~88mm) and for typical ring currents of about 200mA this results in a total incident power of ~92 W at the CLS beamline and ~35 W at the CAMD wiggler.

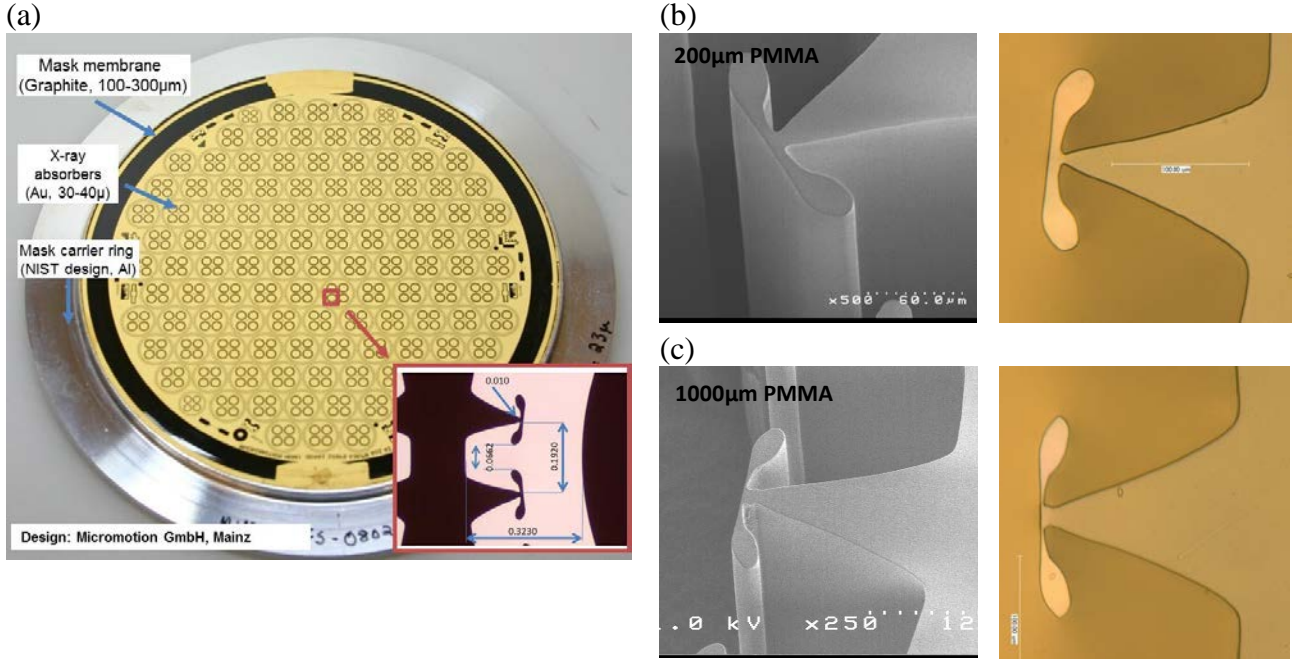


Figure 1 :

(a) Picture of graphite substrate mask (thickness  $\sim 230\mu\text{m}$ ) structured with micro-gears ( $\sim 40\mu\text{m}$  thick gold) and mounted on to Aluminum NIST ring. Patterned area is  $\text{Ø}\sim 88\text{mm}$ . (b) Picture of  $200\mu\text{m}$  tall PMMA structure exposed with x-ray from CAMD bending magnet light source. (c) Picture of  $1000\mu\text{m}$  tall PMMA structure exposed with x-ray from CAMD wiggler light source.

Due to the harder spectrum of the CLS source and the finite thickness of the Au absorber ( $\sim 30\mu\text{m}$ ) only about 90% of the radiation will be blocked in the absorber compared to about 98% at the CAMD wiggler. In case the CAMD wiggler beamline only low Z material absorption filter can be used to tailor the spectrum and reduce the incident power while the CLS beamline also offers a chopper to reduce power (2 modes, 10% and 25%) without changing the exposure spectrum [12].

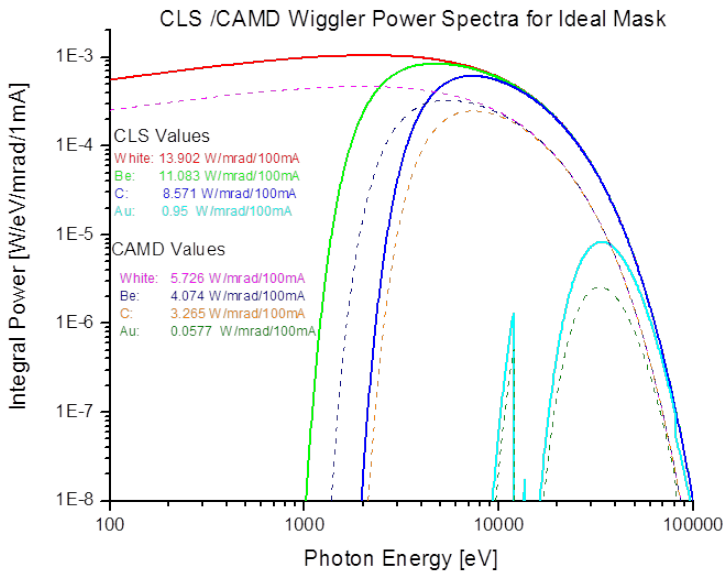


Figure 2:

Power spectra of CLS bending magnet (BM) and CAMD wiggler beamlines.

Besides the spectra generated by the sources additional spectra are calculated after passing Be vacuum window (Be), graphite x-ray mask substrate (C), and gold absorber (Au). The calculated integral power after each absorber is shown in the graph, too. The difference between total power passing the graphite mask (C) and the (Au) is the amount of energy absorbed in an ideal mask per mrad of horizontal beamwidth in the plane of the mask.

1mrad at CAMD wiggler = 1.63cm width

1mrad at CLS BM = 1.62cm width

In order to further understand the effect of heat load and quantify the temperature increase it is necessary to measure the temperature and temperature distribution in a typical mask-substrate assembly during exposure. In Figure 3 the typical setup for standard x-rays lithography exposure experiments in a Jenoptik scanner is shown (both beamlines are equipped with DEX3 scanners from Jenoptik, Jena, Germany). The mask-substrate assembly consists of graphite mask with thick gold absorber and substrate (typically silicon wafers) with thick resist coating (PMMA, SUEX, mr-X) clamped together in the scan stage fixture using proximity shims/spacers defining a gap between them (typical gap width is ~300µm to ~1mm). Mask clamping ring (Al, steel) and wafer holder are water-cooled and kept at 18°C (set chiller temperature). The entire scanner chamber is filled with ~100mbar He atmosphere also kept at 18°C during exposure accounting for negligible absorption losses and effective convective cooling [8,9].

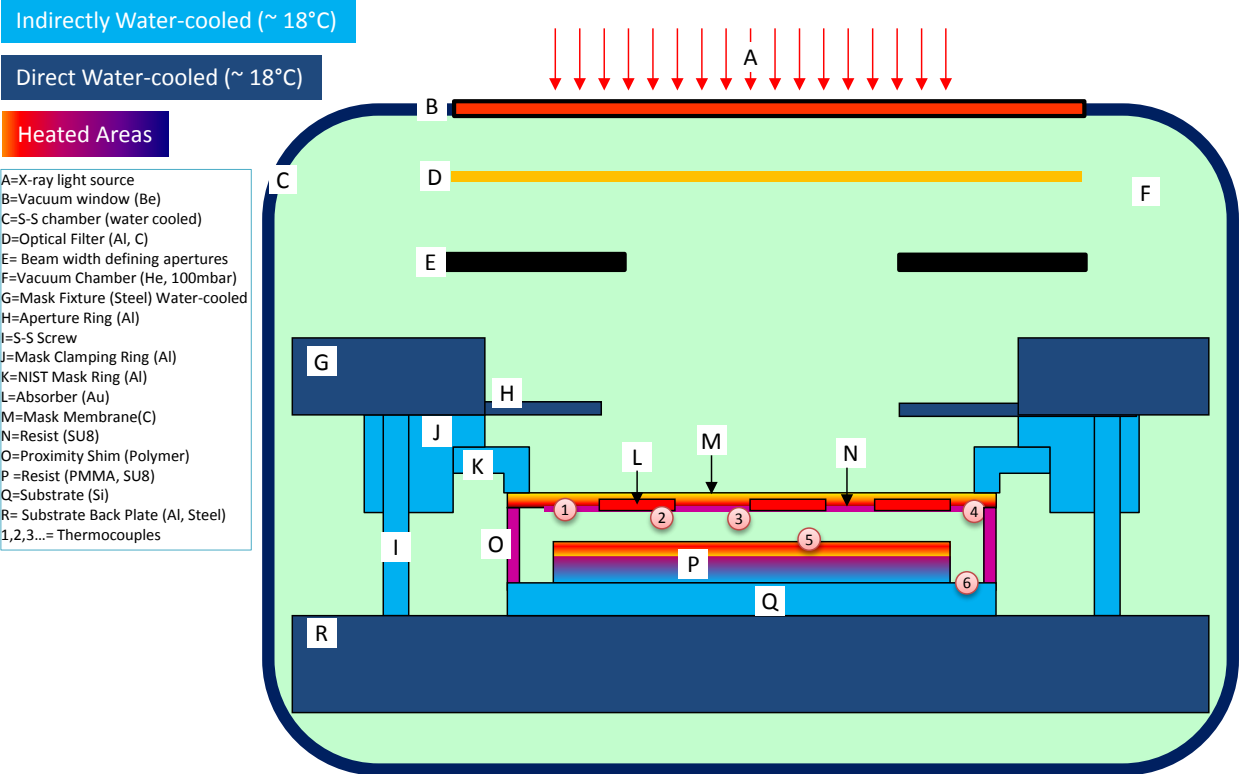


Figure 3:  
 Cross sectional view of mask-substrate assembly for standard x-ray exposure at CAMD and CLS. The thermal couples (TCs) placed in the mask-substrate stack allow temperature monitoring during regular exposures.

Temperature measurements are done using bid size thermocouples (TCs, Omega Engineering Inc, K-Type 5SC series with Ø 76µm, beaded) that are attached with self-gluing Kapton tape to the mask and substrate as shown in Figs. 3,4. Data acquisition is possible with a sample rate of 9Hz allowing to taking temperature data points every ~100msec.

## Experimental Details

Typical thermocouple locations are displayed in Figs. 4. TCs are placed on Au absorber to prevent direct heating from absorption of the synchrotron beam. The different TC locations allow measurements of 2D temperature distribution under thermal load/exposure.

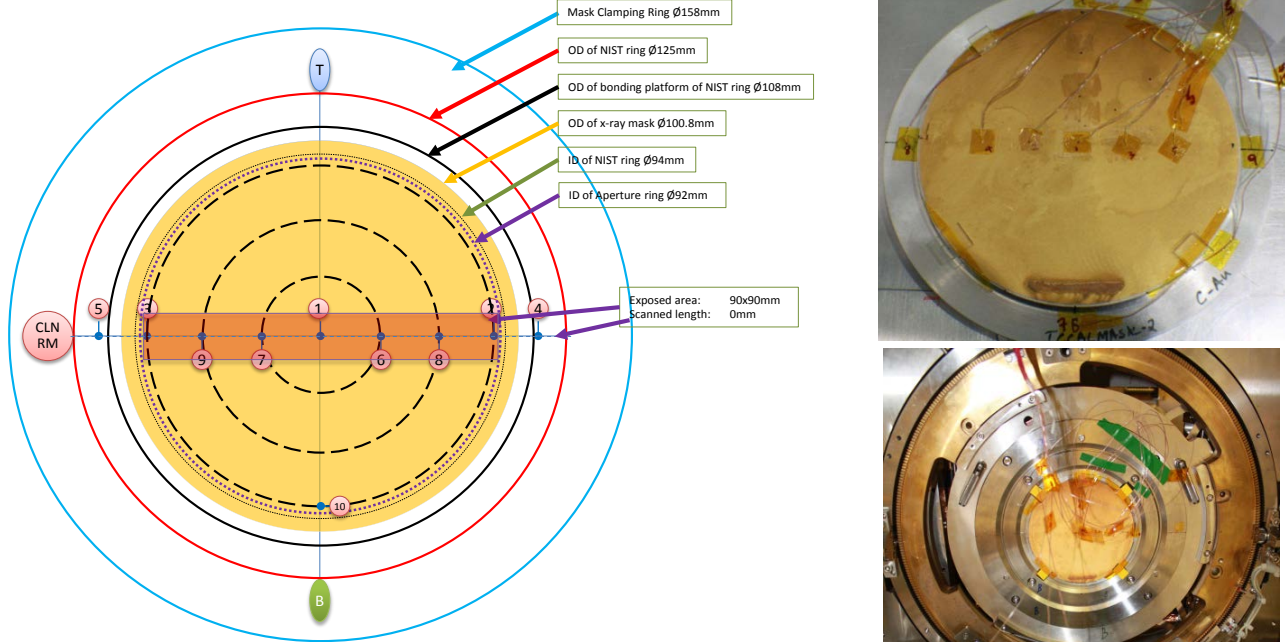
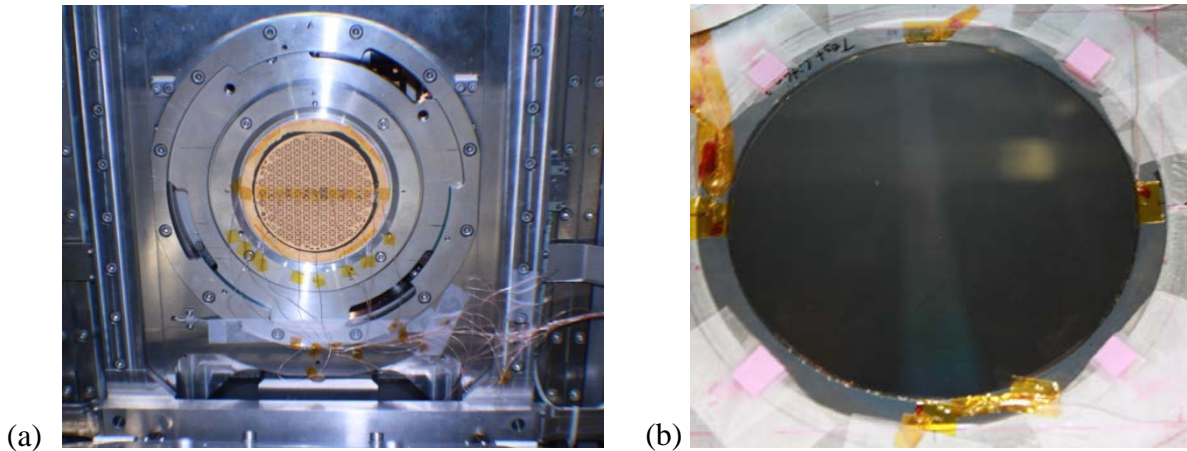


Figure 4:

Schematic above is showing locations of TCs attached to x-ray mask and substrate. Pictures to the right illustrate the real situation for the ideal mask (this mask is fully covered with gold = 100% absorption, top) and after assembly of mask and substrate (Si wafer) onto the DEX3 scanner stage at CLS before closing the flap and clamping them together.

Besides using an ideal mask and substrate (Si wafer with no resist = most effective cooling) measurements for LIGA exposures were conducted with the microgear mask (Fig. 1a) and 1mm thick PMMA on Si wafer as illustrated in Figs. 5a,b.



Figures 5: (a) Microgear mask equipped with TCs mounted into CAMD DEX3 scan stage, (b) Silicon substrate with 1mm thick PMMA resist and TC's attached to the substrate. Pink plastic shims define a proximity gap of about 500µm between mask plane and top of the resist.

## Thermal Modeling

Studies reported in [8] derived with a detailed model for heat transfer between mask, resist, wafer substrate and the surrounding fixtures taking into account heat transfer through convection, conduction and radiation. In our studies a lumped heat model was developed combining all effects and interfaces assuming that the temperature differences inside each lump (mask, substrate/resist) is negligible. The equation below represents our model and connects it with experimental data derived from our experiments. Simulations of exposures were only done for a completely covered Au mask (ideal mask) and a Silicon substrate without resist placed relative to the mask at 2.8 mm proximity gap.

$$q = mc_p \frac{\Delta T_1}{\Delta t} = hA\Delta T_2$$

With:

$q$  = Heat load calculated from source

$m, C_p$  = Mass and thermal capacity of substrate material

$\Delta T$  = Substrate temperature increase (measured)

$\Delta t$  = Time to reach steady state (measured)

$h$  = Effective heat transfer coefficient

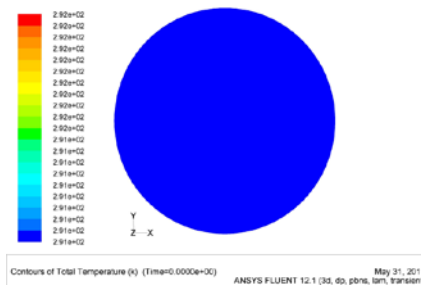
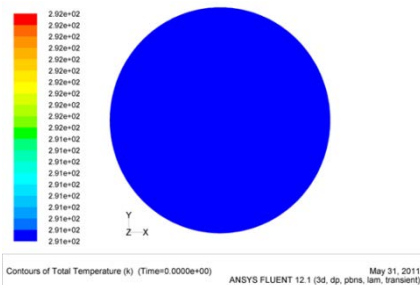
$A$  = Common area between mask and substrate

$\Delta T_2$  = Steady state temperature difference between mask and substrate (measured)

From experiments with different gaps (Table 1) and different ring currents (meaning different heat load) the calculated values for  $h$  are approximately constant for a ~ factor 2 different load but clearly differ between different setups suggesting that a larger gap allows more effective heat exchange/cooling of the surfaces.

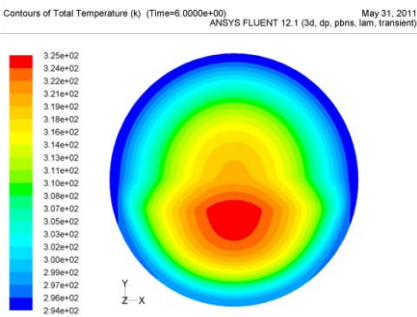
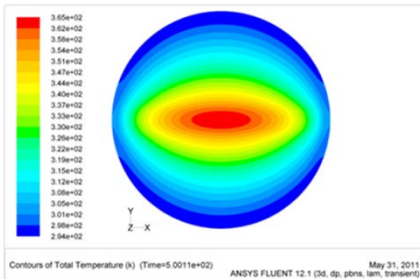
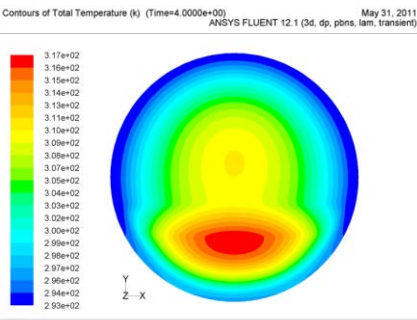
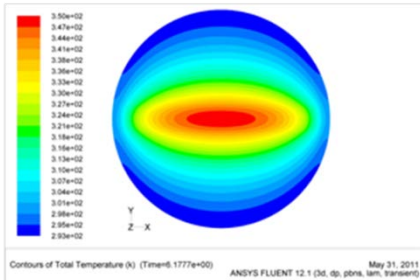
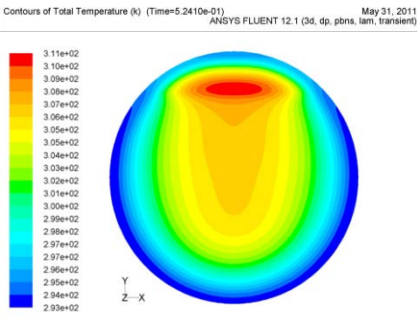
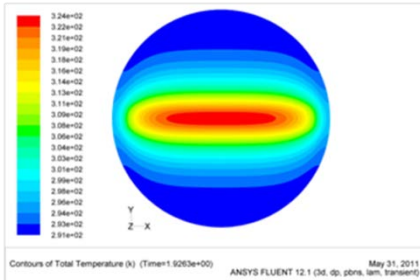
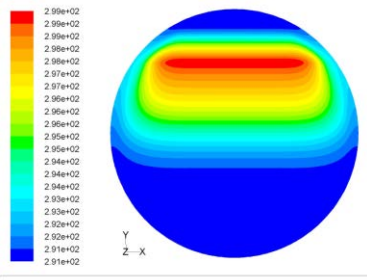
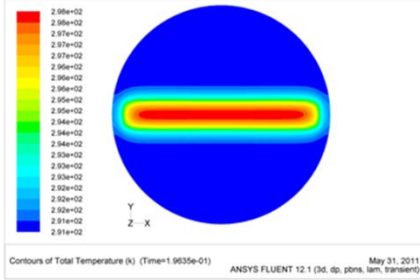
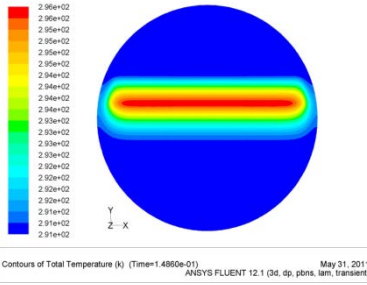
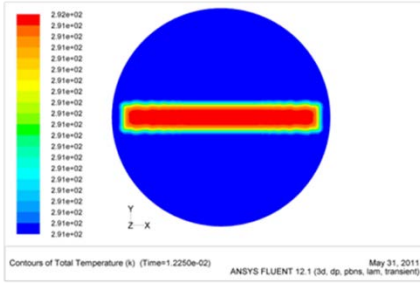
Substrate	Gap	Current	$h$
Si	820 $\mu$ m	107	13.6 W/m <sup>2</sup> K
Si	820 $\mu$ m	183	14.2 W/m <sup>2</sup> K
Si	2.8mm	86	20.6W/m <sup>2</sup> K
Si	2.8mm	166	21 W/m <sup>2</sup> K

The simulation results for stationary and scanned exposures as a function of exposure time (meaning the time after the beam started hitting the assembly) are shown and discussed in Fig. 5.



Initial situation

Mask is in thermal equilibrium with environment



Stationary exposure

Scanned exposure

Figures 5: Results from temperature simulation for different exposure modes.

Open shutters produces a hot line where the beam hits the mask and is absorbed. In the case of scanning motion this line will be somewhere on the mask depending on the scan velocity.

Stationary: After about 0.2 sec a gradient profile begins to develop.

Scan: gradient profile spreads across the upper half of the mask after about 0.5 sec

The previous trends continue for both situation.

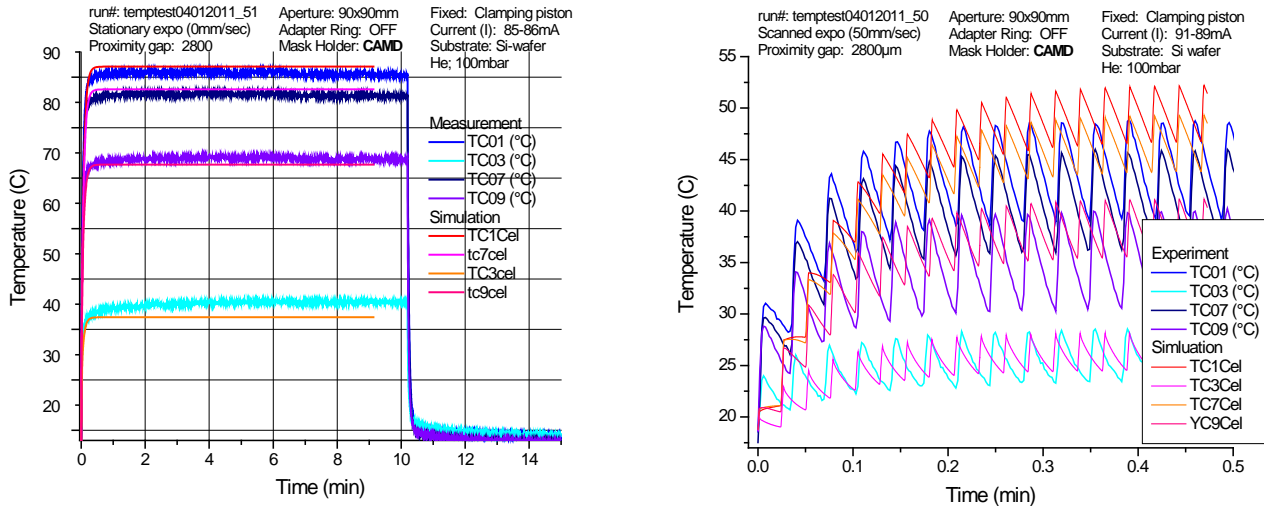
Stationary:

After about 6.2 sec the distribution is almost steady state as there is no significant change to the situation after 50sec. While the mask ring stays at cooling temperature in the turning points it slightly warms up in the horizontal plane where the beam reaches close to it.

Scan:

The distribution correlates with the scan motion and is not reaching a steady state but moves across the mask with the beam/scan location. The maximum temperature difference on the mask is lower for scanned exposures and suggests that thermal load and maximum temperature can be somewhat controlled by the scan velocity [11, 13].

Comparison between experiment and simulation for both cases is shown in Figs. 6 for some of the thermal couples. The stationary case shows a very good match between experiment and simulation proving the quality of the simple model. The noticeable difference for TC 9 is likely caused by experimental uncertainty (fixation and contact of TC). While the general agreement between experiment and simulation is also documented for the scanning mode there is a phase shift that results from the incomplete model not taking into account that the beam is blocked and not hitting the substrate while in the turning points. This also explains that the temperature increase for the experimental data is slower than predicted by the model as the substrate/mask assembly has some time to cool down further as the beam is not permanently 'on'. For a more accurate modeling the exact scanning motion needs to be considered.



Figures 6: Comparison of experiment and simulation of temperature increase on the x-ray mask for stationary (left) and scanning (right) exposures.

## Results

### Temperature Measurements

Experiments have been conducted at both beamlines (CLS, CAMD) with varying conditions and setups. Some typical results are shown and briefly discussed in the following text. In Figures 7 results from preliminary studies using a special TC setup (Fig. 7a) indicate that the cooling of mask and substrate fixture is not ideal. TCs located in positions 2-5 are not exposed to the beam but are heated only from the mask (ideal mask). The findings indicated that waterflow in the cooling circuit was blocked. After repair the temperature increase was reduced to maximum 2°C at full heat load.

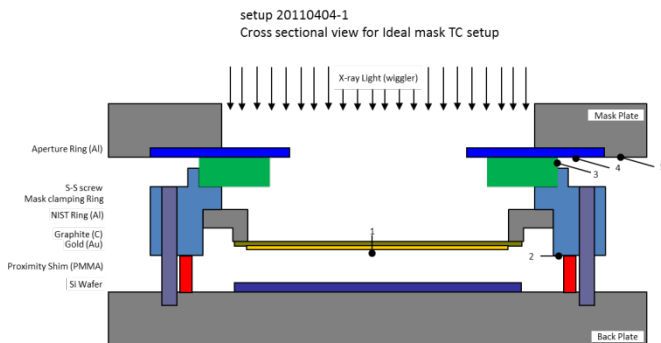


Fig. 7a: Setup of thermocouples for basic experiments.

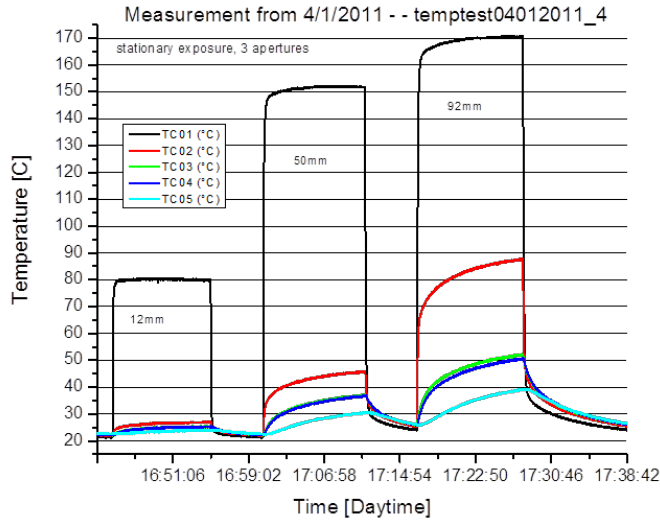


Figure 7a:

Stationary exposure CAMD wiggler, I ~150mA, only mask – large gap to water-cooled substrate fixture

Use of different horizontal aperture width reduces total power impinging onto the mask resulting in different increase of temperature.

For large beam width the beam gets close to the mask ring and mask fixture leading to a significant temperature increase in the fixturing suggesting that cooling through the water-cooled fixture was not perfect (flow was blocked and after repair max. increase was below 2°C).

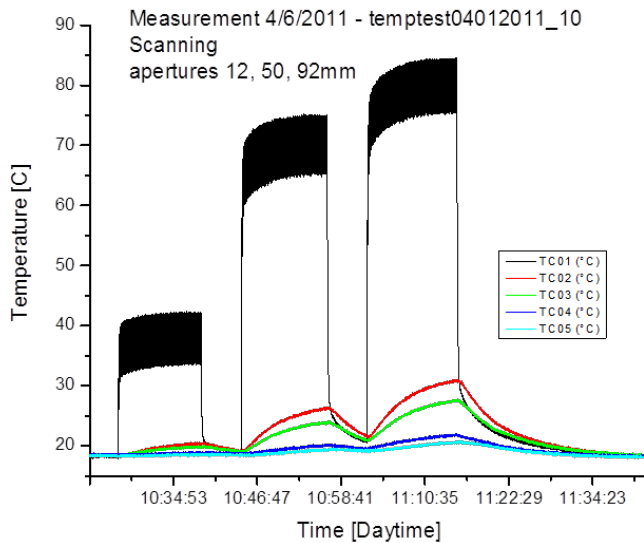


Figure 7b:

Scanning exposure (velocity 50mm/sec) CAMD wiggler, I ~135mA, only mask – large gap to water-cooled substrate fixture

Use of different horizontal aperture width reduces total power impinging onto the mask resulting in different increase of temperature.

Observation match the stationary exposure. For approximately same ring current (=thermal load) the maximum temperature is significantly lower.

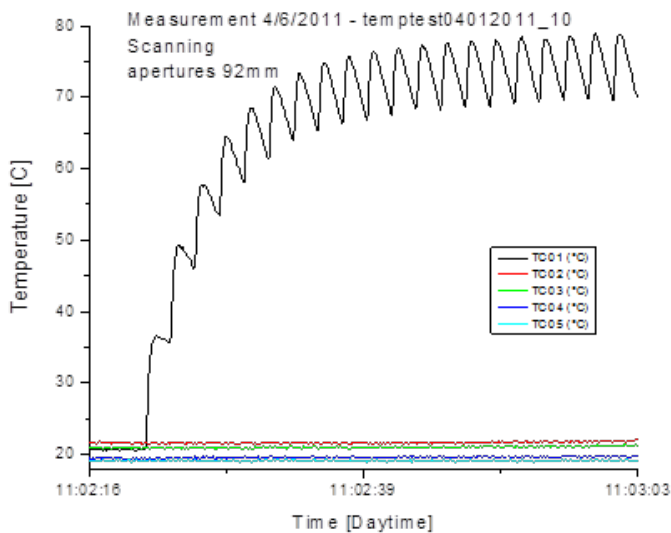


Figure 7c:

Close up of Fig. 7b of the early stage when the 92mm wide beam hits the mask. Temperature quickly increases and reaches almost steady state in about 1min (TC in mask center, TC1). The presence of the beam is clearly felt by TC1 indicated by the temperature modulation of about +/- 7°. Due to the low thermal mass of the free-standing mask substrate temperature changes occur very fast.

Figure 8 summarizes some of the systematic measurements accounting for proximity gap, substrate material and He pressure.

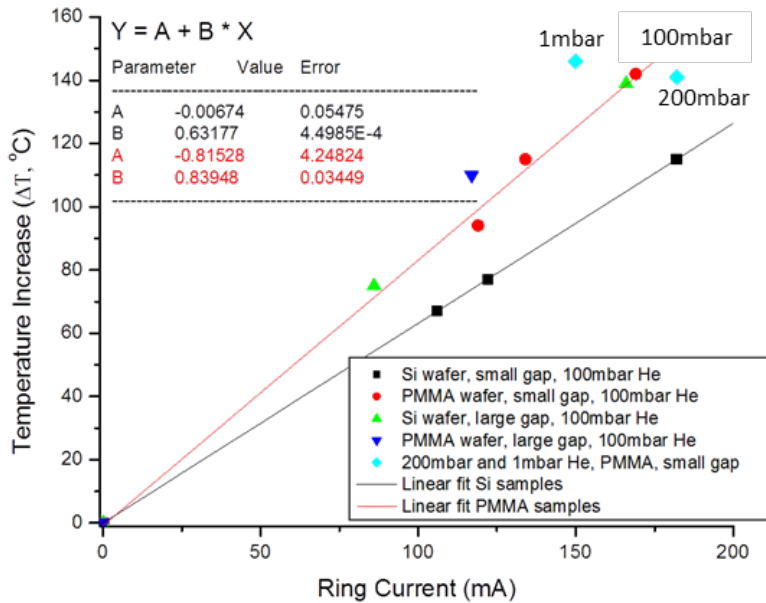


Figure 8:

Temperature increase measured with TC1 and an ideal mask under varying conditions.

Silicon wafer substrate without resist and smallest gap results in lowest rate of temperature increase of about 0.6° C/mA. Replacing the substrate with a 1mm PMMA wafer the rate increases to about 0.8° C/mA proving the insulating effect of the polymer/resist. Increasing the gap for both settings results in larger rates (PMMA more a trend, Si very clearly) suggesting that proximity gap and substrate cooling for the mask matters. He atmosphere also has an effect – 200mbar supports cooling while 1mbar allows higher temperature increase.

Figures 8c,d show the temperature increase on the ideal mask and silicon wafer substrate with the TC arrangement illustrated in Fig. 8a,b for stationary and scanning exposures at the CLS source. Due to the higher radiation power the increase is significant especially in the center of the mask and cannot be accepted in lithography exposures. It should be noted that for the stationary exposure TCs 1 and 5 show about the same temperature increase as they are both placed in the center of the impinging beam. TC8 which has the same distance to the mask center than TC5 but is outside the actual beam shows a significantly lower temperature indicating that heat conduction in the mask substrate is limited and convective cooling via the He atmosphere very effective.

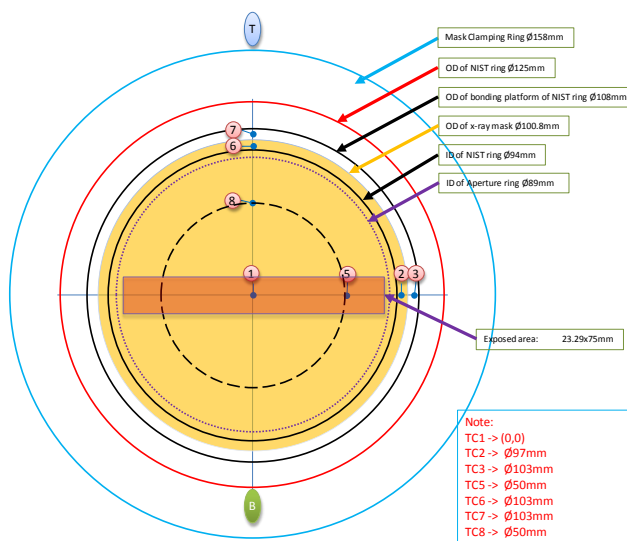


Fig. 8a: Location of TCs mounted on x-ray mask.

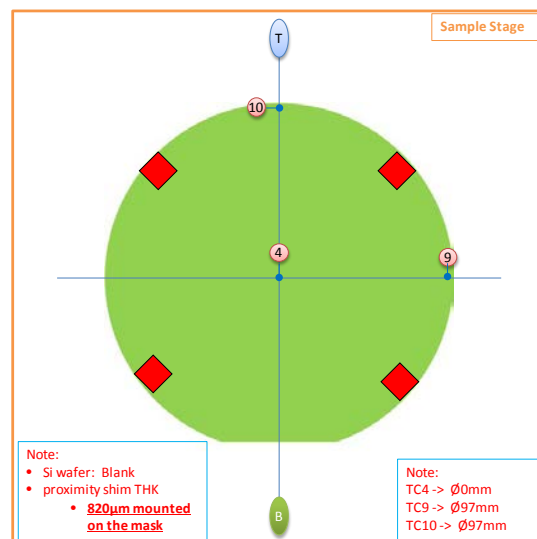


Fig. 8b: Location of TCs mounted on substrate.

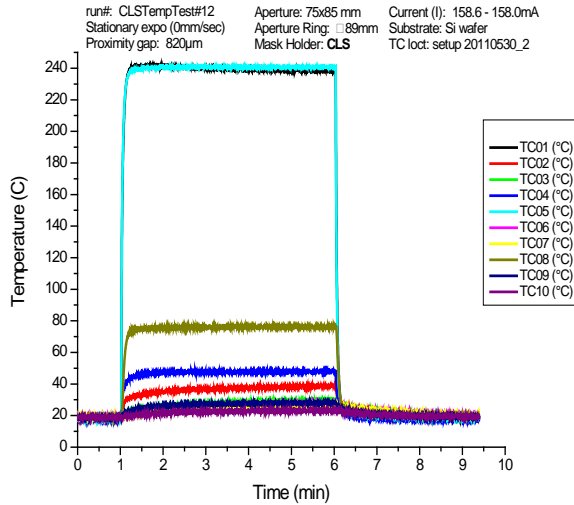


Fig. 8c: Temperature increase at CLS beam line (ideal mask, small gap, Si substrate) for stationary exposure.

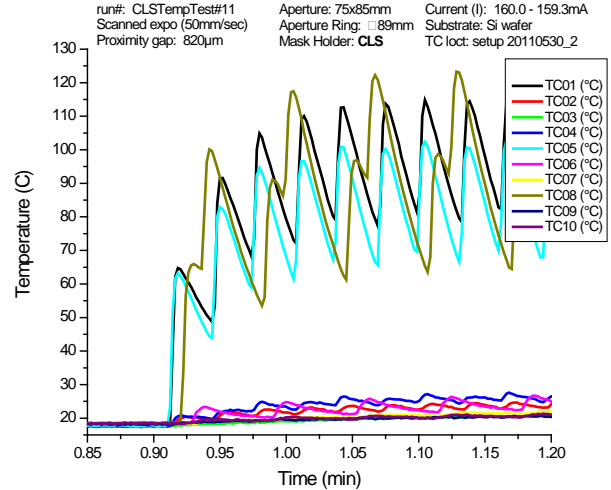


Fig. 8d: Temperature increase at CLS beam line (ideal mask, small gap, Si substrate) for scanning exposure.

In the CLS beamline a rotating wheel (chopper) allows periodic blanking of the beam for a certain time thereby reducing the heat load without changing the exposure spectrum. In Figures 9a,b the effect of the chopper on temperature increase is illustrated for experimental conditions comparable to the runs shown in Fig. 8. The chopper duty cycle is 10% meaning that the beam is passing the chopper only 10% of the available exposure time. The effect is clearly documented – the maximum temperature increase in the center of the mask drops from about 250°C to only 42°C.

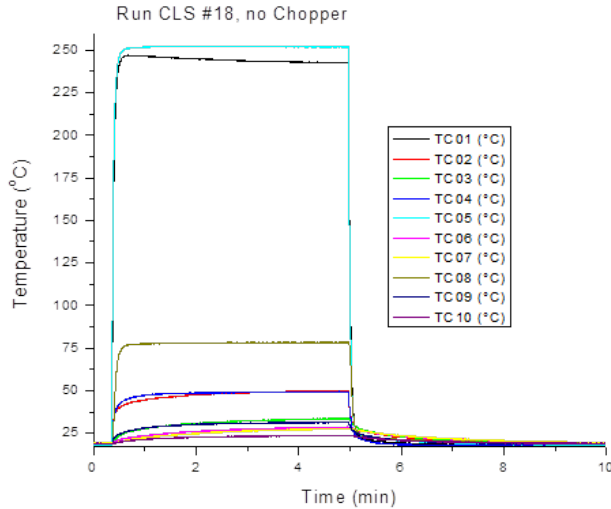


Fig. 9a: Temperature increase at CLS beam line (ideal mask, small gap, Si substrate) for stationary exposure.

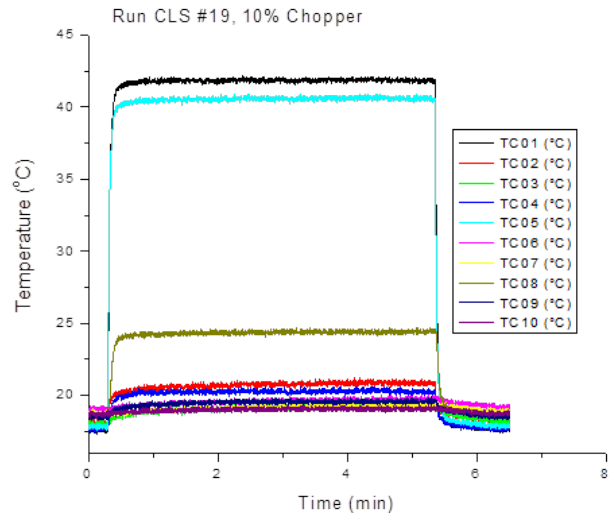


Fig. 9b: same as experiment shown in Fig. 9a but with chopper running at 10% duty cycle.

## Lithography Results

Lithography tests have been performed with a microgear mask (see Fig. 1) and thermocouples placed on mask and substrate in the outside areas to not compromise the pattern transfer. Figures 10a,b document the location of the TCs on the mask and substrate, respectively. Proximity gap was set to ~800µm between the mask plane and the top of the 1mm thick PMMA resist glued onto

silicon wafer covered with a  $\text{TiO}_2$  seed layer. Figures 10c-f illustrates some of the channels and the temperature changes recorded during the exposure. The measurements demonstrate that a maximum temperature increase by  $10^\circ\text{C}$  to about  $30^\circ\text{C}$  is measured on the mask while the substrate only measures a  $2^\circ\text{C}$  temperature rise. The beam motion is recognized as temperature change and results in a modulation of the temperature during exposure. Turning points see a larger temperature change as the beam is only passing by once per scan cycle allowing for longer time to cool down.

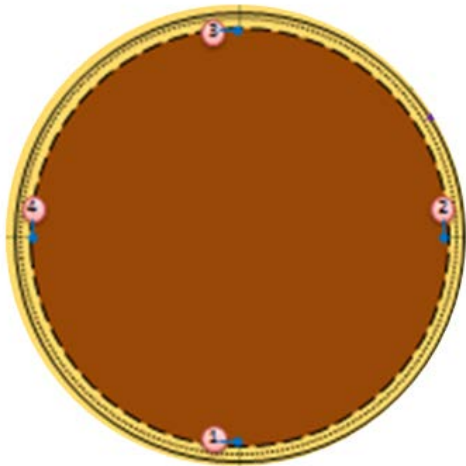


Figure 10a: Location of TCs attached to the gear x-ray mask. Scan direction is between TC2 and TC3.

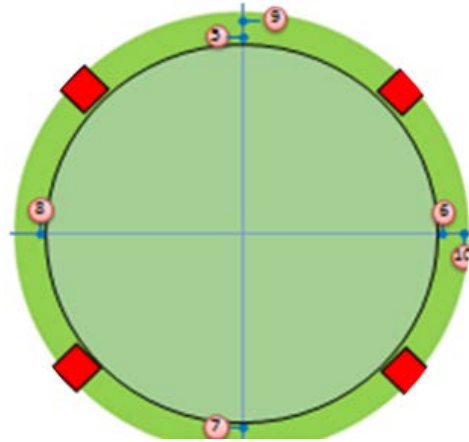


Figure 10b: Location of TCs attached to the substrate. Scan direction is between TC7 and TC5/9.

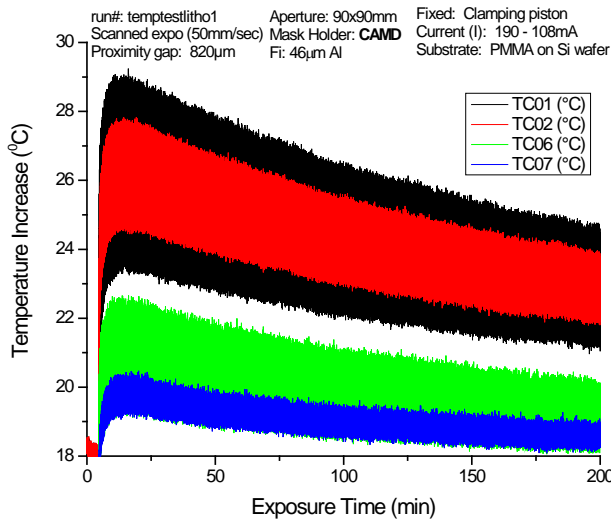


Figure 10c: Temperature recording of sample Litho1, exposed at high ring current at the CAMD wiggler beamline. Absorption in a  $46\mu\text{m}$  thick Al filter is reducing the thermal load. TCs1&2 are mounted on the mask, TCs6&7 on the substrate in a turning point and on the center line, respectively. The temperature reaches a maximum and continuously drops with decreasing ring current.

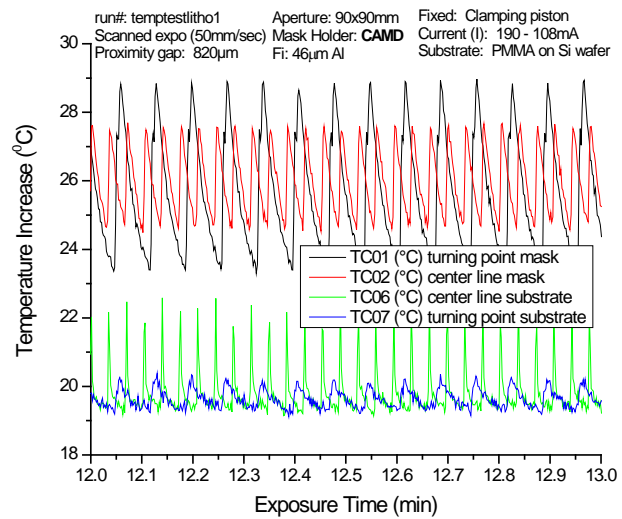


Figure 10d: Close up of Fig. 10c after reaching thermal equilibrium ( $\sim 12\text{min}$  into the exposure). Temperature changes in turning points are higher compared to the center line location as the beam passes by only once per scan cycle allowing for a longer cooling period. The peak-like jump of TC6 suggests that a part of the TC is 'seeing the beam'. Substrate cooling is efficient with a temperature increase of  $\sim 2^\circ\text{C}$  above cooling temperature. The mask ring sees a temperature increase of maximum  $10^\circ\text{C}$ .

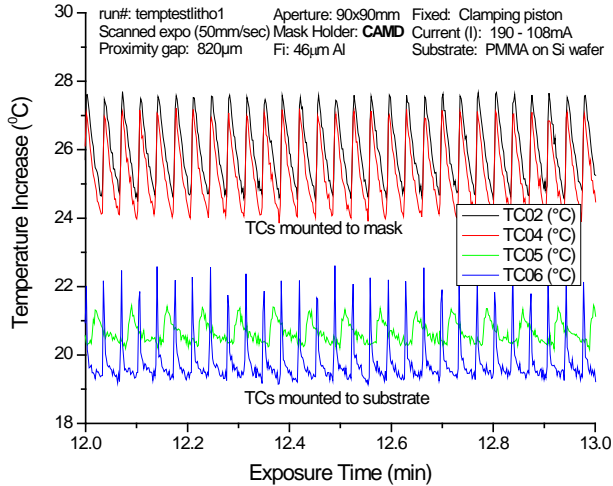


Figure 10e: Close up of Fig. 10c after reaching thermal equilibrium (~12min into the exposure). TCs mounted on the mask show a higher increase than on the substrate in comparable locations indicating that substrate cooling is highly efficient.

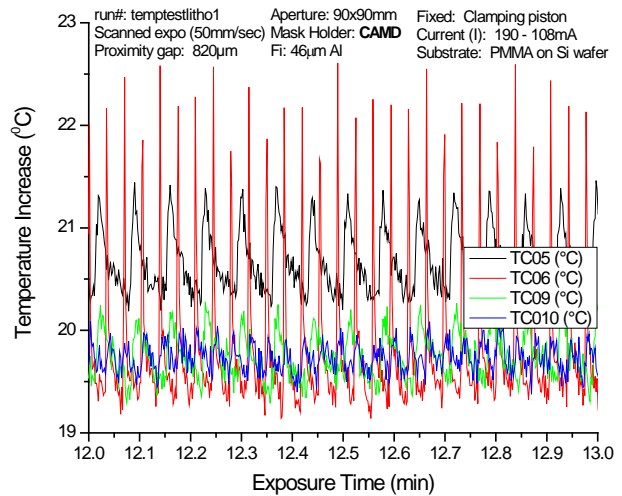


Figure 10f: Close up of Fig. 10c after reaching thermal equilibrium (~12min into the exposure). TCs are mounted on the substrate. Pairs (TC 5,9), (TC 6,10) are close by each other with one close to the open mask area while the other is mounted on the mask ring. The peaks prove that the presence of the beam is clearly 'felt'.

In a 2<sup>nd</sup> lithography experiment an identical setup was exposed at low ring current and with no Al filter (Figures 11a,b). The maximum heat load is comparable for both exposures and similar temperature changes are measured. Expectation is that patterning results will be comparable, too, as is documented in Figures 12. The conclusion for the CAMD exposures is that with proper power control (keeping the maximum temperature increase to 10°C on the mask ring) acceptable lithography results are possible. Note that temperatures have not been measured in the open mask area allowing to use TCs for monitoring purposes and quality control during standard exposures.

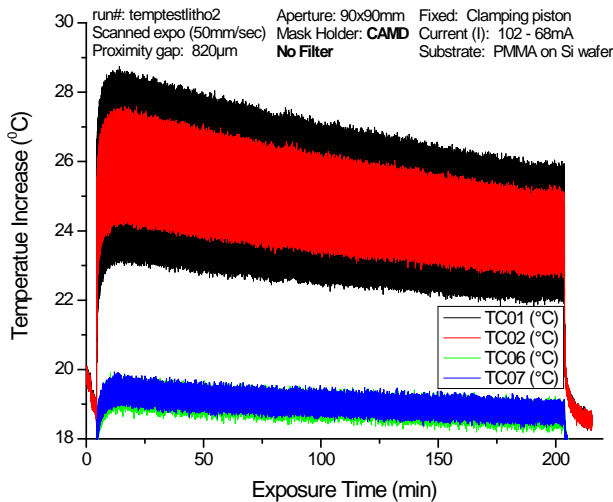


Figure 11a: Temperature recording of sample Litho2, exposed at low ring current at the CAMD wiggler beamline with no filter. TCs1&2 are mounted on the mask, TCs6&7 on the substrate in a turning point and on the center line, respectively. The temperature reaches a maximum and continuously drops with decreasing ring current but at a slightly slower rate as the stored electron beam has a longer lifetime at lower currents.

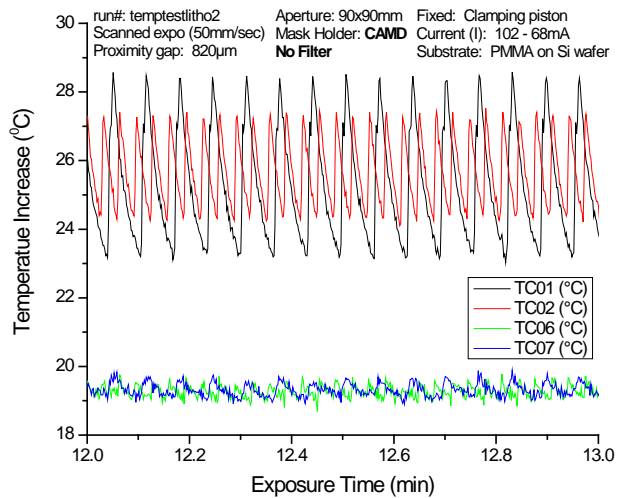
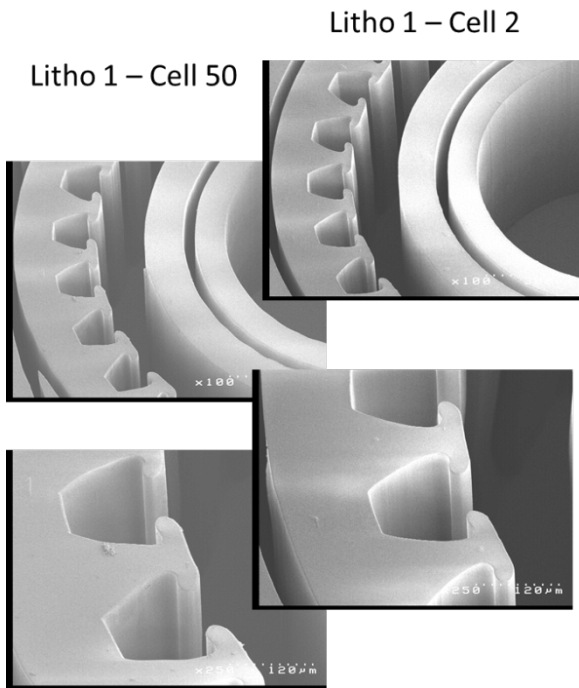


Figure 11b: Close up of Fig. 11c after reaching thermal equilibrium (~12min into the exposure). Results are comparable to Fig. 10d and comments are similar. The substrate modulation is not showing a sharp peak demonstrating that TC6 is placed a little further away from the beam.



CAMD

Figure 12a: Lithography results Litho 1 showing no signs of pattern distortion. Smallest features of the PMMA pattern are  $\sim 10\mu\text{m}$  with a structure height of  $\sim 1\text{mm}$ . Cell 50 is located in the center of the mask, cell 2 close to a turning point.

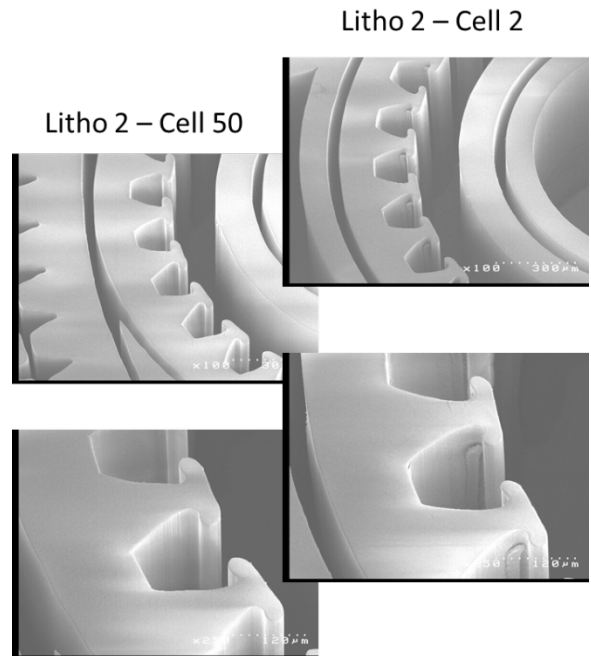


Figure 12b: Lithography results Litho 2 showing no signs of pattern distortion. Cell 50 is located in the center of the mask, cell 2 close to a turning point.

In a first exposure test similar samples have been exposed at the CLS SyLMAND beamline. The TC location is comparable with the CAMD tests (see Figure 8a,b) and the results are shown in Figures 13a,b. Using the chopper at 25% duty cycle and no filter results in negligible temperature rise of maximum  $2^\circ\text{C}$  while the use of a  $30\mu\text{m}$  thick Al filter increases the temperature by about  $10^\circ\text{C}$  to almost  $30^\circ\text{C}$ .

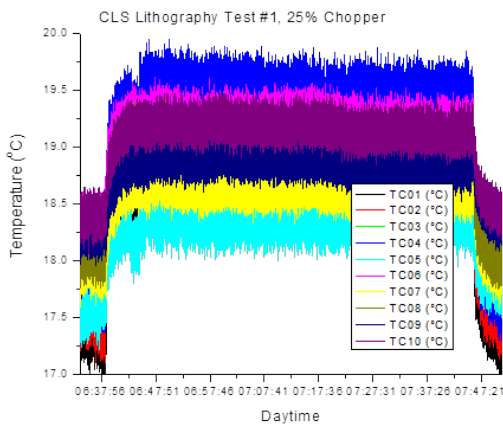


Figure 13a: Lithography test 1 with 25% chopper and no filter at CLS SyLMAND beamline.

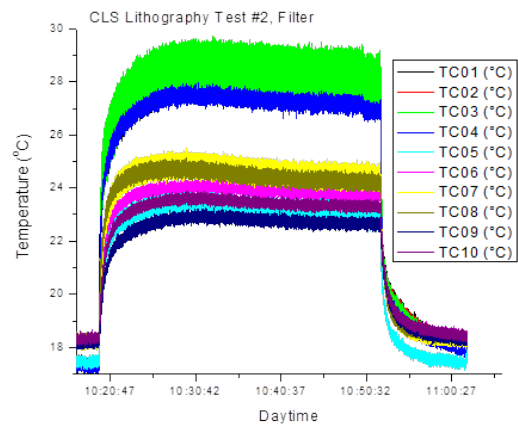


Figure 13b: Lithography test 2 with  $30\mu\text{m}$  Al filter and no chopper at CLS SyLMAND beamline.

Patterned structures for both tests are shown in Figures 14 and demonstrate that by controlling the temperature increase even at a very high power beamline excellent lithography results can be achieved. It is notable that the temperature reducing effect of the chopper is dramatic though it comes with a price of longer exposure time.



Figure 14a: Optical micrograph of 1mm tall PMMA gear in cell 50 (center of the mask) exposed **with 25% chopper and no filter** at CLS SyLMAND beamline (test 1).



Figure 14b: Optical micrograph of 1mm tall PMMA gear in cell 50 (center of the mask) exposed **with 30µm Al filter, no chopper** at CLS SyLMAND beamline (test 2).

## Conclusions and Future Experiments

An experimental method has been tested to measure temperature changes during x-ray lithography experiments at high power light sources. Thermocouples placed onto the mask and substrate as well as the fixtures provides 2D information about temperature changes occurring during exposure and help with identifying ‘hot’ spots. A simple lumped model accurately describes the temperature response for typical heat loads and will be used in the future to optimize exposure conditions. By keeping the maximum temperature on the mask ring to about 30°C distortion-free copying of fine gear structures into 1mm thick PMMA resists is possible. Reducing the impinging photon flux with filters or chopper ensures good power and spectrum control and leads to accurate lithography results.

## References

- 
- [1] D. Yemane et al.; *Investigation of Heat Load in High Power Wiggler Exposures at CAMD and BESSY*, Proc. HARMST 2009, Saskatoon, Canada (2009), 65-66.
  - [2] D. Yemane et al.; *Heat Load Experiments at CAMD and CLS*, Proc. HARMST 2011, HsinChu, Taiwan (2011), 40-41.
  - [3] G. Feiertag et al.; *Thermoelastic deformations of masks for deep x-ray lithography*, Microelectronic Eng. 27 (1995), p. 513-516.
  - [4] M. Neumann et al.; *Heat transport in masks for deep X-ray lithography during the irradiation process*, J. Microelectronics, Vol. 28, Issue 3 (1997), 349-355.
  - [5] F. Pérennès et al.; *Microstructures deformations due to heat load problems in deep X-Ray lithography*, Proc. XXX Convegno Nazionale dell' AIAS, Sept 2001, 1351-1358.
  - [6] S. Achenbach et al.; *Numerical simulation of thermal distortions in deep and ultra deep x-ray lithography*, Microsystem Technologies, Vol 9, Issue 3 (2003), 220-224

- 
- [7] Y. Utsumi et al.; *Large area and wide dimensions X-ray lithography using energy variable synchrotron radiation*, Microsystem Technologies, Vol 13, Issue 5 (2007), 417-423.
- [8] A. Ting; *Temperature Rise of the Mask-Resist Assembly during LIGA Exposures*; Sandia report SAND2004-5446 (2004): <http://prod.sandia.gov/techlib/access-control.cgi/2004/045446.pdf>.
- [9] F.J. Pantenburg; *Instrumentation for Microfabrication with Deep X-ray Lithography*; AIP Conf. Proc. **879** (2007):1456-1461.
- [10] V. Nazmov et. al.; *Investigation of the radiation-induced thermal flexure of an x-ray lithography mask during a tilted exposure*; J.Vac.Sci.Technol. B **29** (2011):011007-1 – 011007-9 <http://dx.doi.org/10.1116/1.3524905>.
- [11] S. Achenbach et. al.; *Optimierung der Prozeßbedingungen zur Herstellung von Mikrostrukturen durch ultratiefe Röntgenlithographie (UDXRL)*; FZK scientific report 6576, Karlsruhe (2000).
- [12] S. Achenbach et al.; *Synchrotron Laboratory for Micro and Nano Devices – Facility Concept and Design*, Microsystem Technologies, Volume 16, Numbers 8-9 (2010), 1293-1298.
- [13] C. Koerner and W. Seemann; *Thermo-mechanical behaviour of X-ray masks in micro system technology*; PAMM (2009) Volume 9, Number 1, p. 371-372.